



# Cancellation of electron and hole contributions to the Hall effect in ultrathin Bi films grown on GaAs(110)

Naoto Ito , Ryuichi Masutomi, and Tohru Okamoto *Department of Physics, University of Tokyo, 7-3-1 Hongo, Bunkyo-ku, Tokyo 113-0033, Japan*

(Received 14 September 2021; revised 7 April 2022; accepted 19 May 2022; published 31 May 2022)

Magnetotransport measurements have been performed on ultrathin Bi films grown on GaAs(110). While large positive magnetoresistance is observed at low temperatures, the Hall resistance is found to be extremely small. This is explained by the cancellation of contributions of electrons and holes, which are estimated to have close density and mobility values. By analogy with graphene near the charge neutral point, magnetotransport properties are discussed in relation to the formation of Dirac cones.

DOI: [10.1103/PhysRevB.105.205434](https://doi.org/10.1103/PhysRevB.105.205434)

## I. INTRODUCTION

Bismuth (Bi) is one of the most studied elements in solid-state physics because of its unique electronic properties arising from low carrier density, small effective masses, and strong spin-orbit coupling. Recently, great attention has been paid to ultrathin Bi films grown on insulating substrates. The rhombohedral (111) single bilayer was predicted to be a two-dimensional (2D) topological insulator [1]. The prediction was experimentally verified for a bilayer grown on Bi<sub>2</sub>Te<sub>3</sub>(111) [2,3] and a mechanically exfoliated bilayer [4]. Multilayer films of rhombohedral (111) and their metallic surface states are extensively studied partly in relation to the topological nature of bulk Bi [5–14]. A Dirac-cone feature was predicted at the surface of films consisting of odd numbers of rhombohedral (110) atomic layers [15]. Furthermore, two-monolayer and four-monolayer rhombohedral (110) films were suggested to become 2D topological insulators when they have the black phosphorus structure [16]. Thus, ultrathin Bi films exhibit a variety of novel phenomena in different crystal structures.

Patrin *et al.* have shown that continuous and flat pseudocubic (110) [rhombohedral (1 $\bar{1}$ 0) or (112)] Bi films can be grown on GaAs(110) [17,18]. The scanning tunneling microscopy (STM) measurements at 300 K revealed that orientationally ordered epitaxial films were obtained by deposition at 30 K, while deposition at 300 K produced more three-dimensional films. They also found that the pseudocubic [001] direction of the Bi overlayers was rotated by  $\pm 10^\circ$  from the substrate [1 $\bar{1}$ 0] direction. This was explained in terms of the weakness of the van der Waals interaction between the overlayer and the substrate. On the other hand, the electronic states and transport properties were not studied.

In this paper, we study the magnetotransport properties of ultrathin Bi films produced by low-temperature deposition on GaAs(110) and subsequent annealing to 300 K, following the procedure in Ref. [18]. Positive magnetoresistance, which is attributed to high carrier mobilities, is observed at low temperatures. On the other hand, the Hall resistance is found to be

extremely small. This is explained by the cancellation of contributions of electrons and holes, which are estimated to have close density and mobility values. By analogy with graphene, where similar magnetotransport behaviors are observed near the charge neutral point, we discuss the experimental results in relation to the formation of Dirac cones.

## II. EXPERIMENTAL SETUP AND SAMPLE PREPARATION

The GaAs(110) substrate was prepared by cleaving a non-doped insulating single crystal, which was cooled down to liquid helium temperatures. As shown in Fig. 1, gold electrodes were prepared on noncleaved surfaces in advance. The cleavage of GaAs and the subsequent deposition of Bi films with thickness of 1.8 nm were performed *in situ* in an ultrahigh vacuum chamber immersed in a liquid helium bath. The amount deposited was measured with a quartz crystal microbalance and determined with an accuracy of about 5%. Magnetotransport data were taken in a Hall bar geometry ( $4 \times 0.35 \text{ mm}^2$ ) (see Supplemental Material [19]) using the standard four-probe lock-in technique. The magnetic-field direction with respect to the surface normal was controlled using a rotatory stage on which the sample was mounted, together with a Hall generator, resistance thermometers, and a heater. The sample stage can be cooled to 1.5 K via a silver foil linked to a small pumped <sup>4</sup>He pot and heated to 300 K by the heater. The contact resistance between the ultrathin film and the electrodes is estimated to be less than or comparable to the resistance of the film by subtracting the four-probe resistance from the two- or three-probe resistance. Similar experimental procedures were used to study the transport properties of other 2D materials [20–24].

Figure 2 shows the typical annealing behavior of the sheet resistance  $R_{sq}$  of a 1.8-nm-thick Bi film at zero magnetic field ( $B = 0$ ). Films as-deposited at liquid He temperatures show superconductivity below 4–5 K. This suggests that the films are amorphous, as well as ultrathin Bi films quench-condensed on Ge-coated glass substrate [25]. When the films are heated to 40–60 K,  $R_{sq}$  begins to increase abruptly and

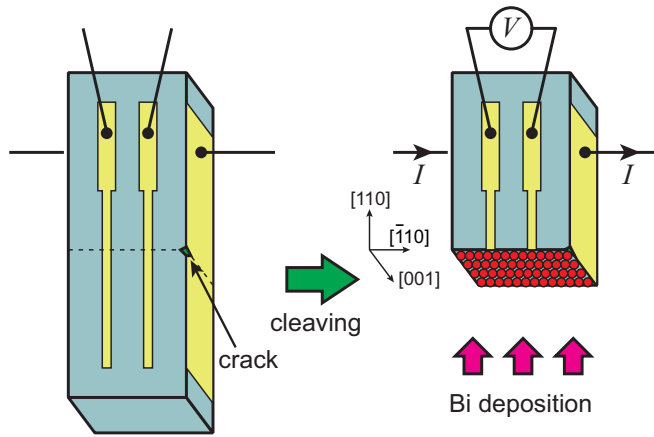


FIG. 1. Schematic view of the experimental setup. Gold electrodes were prepared on noncleaved surfaces in advance. The cleavage of a 0.35-mm-thick GaAs wafer, deposition of Bi films, and magnetotransport measurements were performed *in situ* under low-temperature and ultrahigh vacuum conditions.

irreversibly. Similar behavior has been reported for much thicker quench-condensed Bi films with lower transition temperature ( $\sim 20$  K), and attributed to a structural phase transition from the amorphous to crystalline phase [26,27]. Above the transition temperature,  $R_{sq}$  turns to decrease on further heating with a rate of  $\sim 1$  K/min. The decrease stops after keeping temperature at  $\sim 300$  K for  $\sim 1$  hr. Then the films are cooled down to liquid He temperatures and the magnetotransport properties are studied. After the annealing up to 300 K,  $R_{sq}$  exhibits metallic temperature dependence. Furthermore, as described below, we observe large positive magnetoresistance, indicating the existence of high-mobility carriers. We believe that continuous and flat pseudocubic

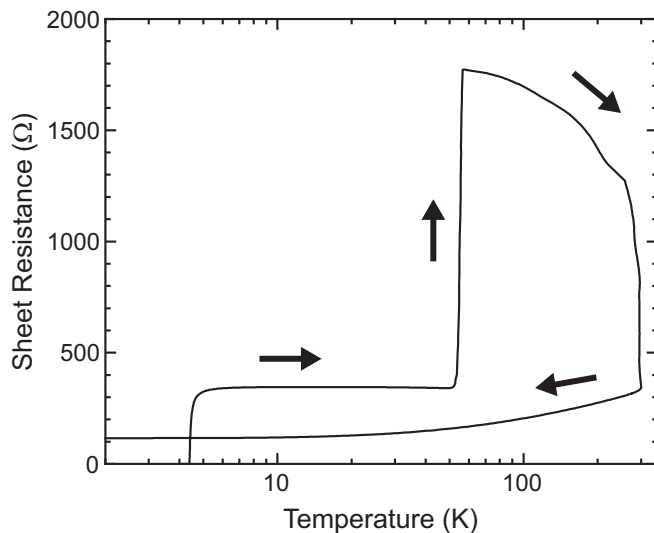


FIG. 2. Typical annealing behavior of  $R_{sq}$  of a 1.8-nm-thick Bi film at  $B = 0$ . Films as-deposited show superconductivity below 4–5 K. The abrupt increase at 40–60 K is attributed to a structural phase transition from the amorphous to crystalline phase. The decrease near 300 K can be understood as a result of improvement of crystallinity.

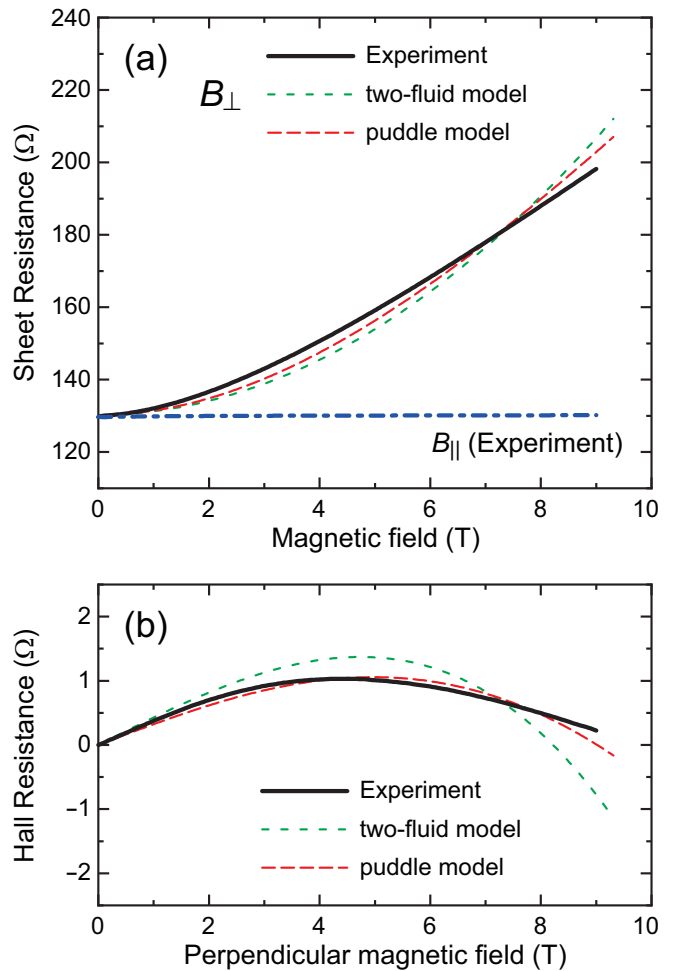


FIG. 3. Magnetic-field dependence of (a)  $R_{sq}$  and (b)  $R_H$  of F1 at 1.7 K. The magnetic field is perpendicular to the film except for the dash-dotted line (blue) representing the parallel-magnetic-field dependence of  $R_{sq}$ . Solid lines are the experimental data. Dotted lines (green) are the fits using Eqs. (1) and (2). Dashed lines (red) are the fits based on Eq. (5).

(110) [rhombohedral ( $1\bar{1}0$ ) or (112)] films, which are similar to those studied by Patrin *et al.* [18], are formed by the two-step growth process, i.e., low-temperature deposition and subsequent annealing to 300 K. In contrast, when the deposition was performed at 300 K, we were not able to produce a conducting film. This is consistent with the STM study of Ref. [18], which reveals that the formation of islands makes the film discontinuous in room-temperature growth. It was also reported in Ref. [18] that low-temperature deposited films become discontinuous when the annealing temperature is increased to 375 K.

### III. RESULTS AND DISCUSSION

In Fig. 3(a), magnetotransport data at 1.7 K on an annealed film (denoted by F1) are presented. The sheet resistance shows strong dependence on the perpendicular magnetic field  $B_{\perp}$ . Since the magnetoresistance is very small in a magnetic field parallel to the film plane, the observed  $B_{\perp}$  dependence of  $R_{sq}$  should be related to the in-plane motion of carriers. We also

performed measurements on a film annealed to only 100 K, which has much higher low-temperature sheet resistance, and found only very small positive magnetoresistance associated with the weak antilocalization correction (see Supplemental Material [19]). We believe that the 2D mobility of carriers is greatly improved by the annealing up to 300 K. The low-temperature values of  $R_{\text{sq}}$  of our films are much lower than those of epitaxial Bi films grown on a Si(111) surface for similar film thickness [7,10]. The Lorentz angle between the drift velocity and the electric field is given by  $\theta_L = \pm \tan^{-1}(\mu B_{\perp})$ , where  $\mu$  is the mobility of carriers and the sign depends on the charge. When all the carriers have the same  $\theta_L$ , the drift velocity is parallel to the current and  $R_{\text{sq}}$  does not depend on  $B_{\perp}$ . In the case of the coexistence of different kinds of carriers, on the other hand, the direction of the drift velocity of each carrier deviates from the current direction and  $R_{\text{sq}}$  increases with  $B_{\perp}$ .

The  $B_{\perp}$  dependence of the Hall resistance  $R_H$  is shown in Fig. 3(b). In our setup,  $R_H$  is positive (negative) when transport is by holes (electrons). In contrast to the large positive  $B_{\perp}$  dependence of  $R_{\text{sq}}$ ,  $R_H$  remains very small [ $|R_H(B_{\perp})| \ll R_{\text{sq}}(B_{\perp}) - R_{\text{sq}}(0)$ ]. This can be explained in terms of the coexistence of electrons and holes having opposite signs of  $\theta_L$ . (The scenario of cancellation of electron and hole contributions to the Hall effect was also supported by electric-field doping experiments; see Supplemental Material [19].) First, we employ a two-fluid model of transport by electrons and holes in a homogeneous sheet. The  $B_{\perp}$  dependence of  $R_{\text{sq}}$  and  $R_H$  is given by

$$R_{\text{sq}} = \frac{1}{e} \frac{(n_e \mu_e + n_h \mu_h) + \mu_e \mu_h (n_e \mu_h + n_h \mu_e) B_{\perp}^2}{(n_e \mu_e + n_h \mu_h)^2 + \mu_e^2 \mu_h^2 (n_e - n_h)^2 B_{\perp}^2}, \quad (1)$$

$$R_H = \frac{1}{e} \frac{(-n_e \mu_e^2 + n_h \mu_h^2) + \mu_e^2 \mu_h^2 (-n_e + n_h) B_{\perp}^2}{(n_e \mu_e + n_h \mu_h)^2 + \mu_e^2 \mu_h^2 (n_e - n_h)^2 B_{\perp}^2} B_{\perp}, \quad (2)$$

where  $n_e$  and  $n_h$  are the areal densities, and  $\mu_e$  and  $\mu_h$  are the mobilities of electrons and holes, respectively [28]. The dotted lines in Figs. 3(a) and 3(b) are fits to Eqs. (1) and (2), respectively. It should be noted that the resistance was found to be almost isotropic (see Supplemental Material [19]), while the films are grown on an anisotropic GaAs(110) surface. According to Eq. (2), the Hall effect becomes weak only when both  $n_e \approx n_h$  and  $\mu_e \approx \mu_h$  are satisfied. (This was confirmed by calculations of  $R_H$  for various combinations of the parameters; see Supplemental Material [19].) They hold true for the parameters used ( $n_e = 3.1 \times 10^{17} \text{ m}^{-2}$ ,  $n_h = 2.6 \times 10^{17} \text{ m}^{-2}$ ,  $\mu_e = 7.9 \times 10^{-2} \text{ m}^2/\text{Vs}$ , and  $\mu_h = 9.0 \times 10^{-2} \text{ m}^2/\text{Vs}$ ). While the condition  $n_e \approx n_h$  is reasonable in semimetals,  $\mu_e \approx \mu_h$  is not expected unless the effective masses of electrons and holes are close to each other. For example, it was reported that  $\mu_e$  is one order of magnitude higher than  $\mu_h$  in 500-nm-thick Bi films [29].

The suppression of the Hall effect has also been observed in graphene near the charge neutral point [30]. It is widely accepted that random potential fluctuations induce electron and hole puddles in a nominally neutral graphene sheet [31,32]. The electron-hole symmetry in the Dirac-cone energy band structure ensures the cancellation of the Hall resistance at the charge neutral point. To demonstrate the possibility of the formation of a Dirac cone in our Bi films, we have performed

tight-binding calculations on pseudocubic (110) [rhombohedral (1 $\bar{1}$ 0) or (112)] bilayers (see Supplemental Material [19]). In fact, Dirac cones are found to be formed for an appropriate range of parameters. It should be noted, on the other hand, that the type of Dirac cone is different from that in graphene. In contrast to the  $K$  and  $K'$  Dirac points in graphene, the Dirac points are located inside the Brillouin zone and their positions depend on the parameters. According to Ref. [33], this type of Dirac cone is classified as an accidental Dirac cone, like that in the 2D organic conductor  $\alpha$ -(BEDT-TTF) $_2$ I $_3$  [34–36]. Moreover, our system is characterized by strong spin-orbit coupling of Bi, which plays an essential role in the formation of Dirac cones. While further studies are needed to verify the correspondence of the model with the real system, we reexamine the  $B_{\perp}$  dependence of  $R_{\text{sq}}$  and  $R_H$  on the assumption that Dirac cones are formed in our Bi films. We also assume the formation of 2D electron and hole puddles and use the model developed for the magnetotransport of inhomogeneous graphene [37]. A macroscopically inhomogeneous film consisting of locally homogeneous electron and hole puddles with areal fractions  $f_e$  and  $f_h = 1 - f_e$  is considered. In each puddle, the 2D conductivity tensor is given by the Drude formula,

$$\sigma_{i,xx} = \sigma_{i,yy} = \frac{n_{\text{loc}}^{(i)} e \mu_i}{1 + \mu_i^2 B_{\perp}^2}, \quad (3)$$

$$\sigma_{i,xy} = -\sigma_{i,yx} = \frac{n_{\text{loc}}^{(i)} q_i \mu_i^2}{1 + \mu_i^2 B_{\perp}^2} B_{\perp}. \quad (4)$$

Here,  $i$  is  $e$  or  $h$ ,  $q_i = \pm e$  is the charge of carriers, and  $n_{\text{loc}}^{(i)}$  is the local carrier density in the puddles. The effective (macroscopic) conductivity tensor  $\sigma_{\text{eff}}$  is calculated using the effective-medium approximation [37–39], where compact circular puddles are assumed to be embedded in an effective medium whose conductivity is calculated self-consistently. The defining equations are given by

$$\sum_{i=e,h} f_i \delta \sigma_i (I - \Gamma \delta \sigma_i)^{-1} = 0. \quad (5)$$

Here,  $\delta \sigma_i = \sigma_i - \sigma_{\text{eff}}$ ,  $I$  is the  $2 \times 2$  unit matrix, and  $\Gamma = -I/(2\sigma_{\text{eff},xx})$  is the depolarization tensor. Then we can determine  $R_{\text{sq}} = \sigma_{\text{eff},xx}/(\sigma_{\text{eff},xx}^2 + \sigma_{\text{eff},xy}^2)$  and  $R_H = \sigma_{\text{eff},xy}/(\sigma_{\text{eff},xx}^2 + \sigma_{\text{eff},xy}^2)$  for given values of  $f_e$ ,  $n_{\text{loc}}^{(e)}$ ,  $n_{\text{loc}}^{(h)}$ ,  $\mu_e$ ,  $\mu_h$ , and  $B_{\perp}$ .

The best fits using the puddle model are shown as the dashed lines in Figs. 3(a) and 3(b). The parameters used are  $f_e = 0.518$ ,  $n_{\text{loc}} = 3.7 \times 10^{17} \text{ m}^{-2}$ ,  $\mu_e = 0.124 \text{ m}^2/\text{Vs}$ , and  $\mu_h = 0.139 \text{ m}^2/\text{Vs}$ . Since a change in  $n_{\text{loc}}^{(e)}/n_{\text{loc}}^{(h)}$  has a similar effect to that in  $f_e/f_h$ , we here put  $n_{\text{loc}}^{(e)} = n_{\text{loc}}^{(h)} = n_{\text{loc}}$  to avoid the arbitrariness. The fits are improved in comparison with the two-fluid model. As in the case of inhomogeneous graphene [30,37,40],  $R_{\text{sq}}$  is observed to increase linearly rather than quadratically with  $B_{\perp}$  for the high- $B_{\perp}$  region. When the electron-hole symmetry is exactly satisfied (i.e.,  $f_e = 0.5$  and  $\mu_e = \mu_h = \mu$ ), Eq. (5) is simplified as

$$\delta \sigma_{e,xx} (\delta \sigma_{e,xx} + 2\sigma_{\text{eff},xx}) + \sigma_{e,xy}^2 = 0, \quad (6)$$

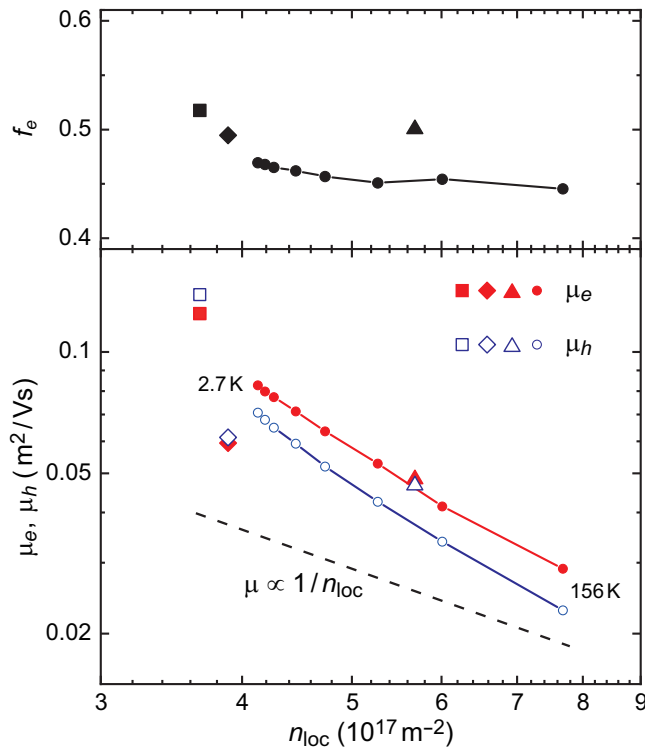


FIG. 4. Plots of  $f_e$ ,  $\mu_e$ , and  $\mu_h$  vs  $n_{\text{loc}}$  obtained using the puddle model. Squares, diamonds, triangles, and circles are for F1 (1.7 K), F2 (1.5 K), F3 (4.2 K), and F4 (2.7, 14, 19, 29, 44, 68, 100, 156 K), respectively. Filled (open) symbols in the lower panel represent  $\mu_e$  ( $\mu_h$ ). The low-temperature resistance of F4 is reproducible after the thermal cycling to 156 K.

with  $\sigma_{\text{eff},xy} = 0$ , so that  $\sigma_{\text{eff},xx}^2 = \sigma_{e,xx}^2 + \sigma_{e,xy}^2$ . The corresponding magnetoresistance is

$$R_{\text{sq}}(B_{\perp}) = R_{\text{sq}}(0)\sqrt{1 + (\mu B_{\perp})^2}, \quad (7)$$

and increases approximately linearly with  $B_{\perp}$  for  $\mu B_{\perp} \gg 1$  [39,40], while  $R_{\text{sq}}$  is proportional to  $1 + (\mu B_{\perp})^2$  in the two-fluid model. The present puddle model is highly simplified and there seems to be much room for improvement, which will reduce the discrepancy from the observed  $R_{\text{sq}}$ . The linearlike positive magnetoresistance, as well as the suppression of the Hall effect, supports the formation of Dirac cones in our systems based on the similarity to inhomogeneous graphene.

Magnetotransport measurements were also performed on other 1.8-nm-thick Bi films (F2–F4). Quantitatively different results were obtained for different films, while the films were produced in the same way and the results were qualitatively similar to each other. The differences may be attributed to small experimental uncertainties of the deposition amount. The inhomogeneity of film thickness and potential fluctuations are expected to become large when the average layer number deviates from an integer value. It is noted that the

1.8 nm thickness corresponds to about 8 monolayers or 4 bilayers in pseudocubic (110) [rhombohedral (110) or (112)] Bi films. The parameters in the puddle model were obtained for each film. In Fig. 4,  $f_e$ ,  $\mu_e$ , and  $\mu_h$  are plotted as functions of  $n_{\text{loc}}$ . For F4, the parameters were also determined for temperatures higher than liquid helium temperatures. As the temperature is increased,  $n_{\text{loc}}$  is enhanced from the low-temperature value, which is related to the strength of film-dependent potential fluctuations. This is probably due to the thermal creation of electron-hole pairs. In all cases,  $R_H$  was found to be very small even at  $B_{\perp} = 9$  T, and  $f_e \approx 0.5$  and  $\mu_e \approx \mu_h$ , which are expected from the electron-hole symmetry, are roughly satisfied. It is found that the mobilities tend to decrease with an increase in  $n_{\text{loc}}$ . The carrier mobility is related to the scattering time  $\tau$  by  $\mu = ev_F\tau/\hbar k_F$ , where  $v_F$  is the Fermi velocity and  $k_F$  is the Fermi wave number. The dominant scattering mechanism in the pure Bi films is likely to be short-range structural defect scattering. In the case of short-range scattering, the scattering time  $\tau$  is inversely proportional to the density of states  $D$ . While  $D$  does not depend on the carrier density  $n$  in a 2D free electron gas, it increases proportionally to  $\sqrt{n}$  in a Dirac-cone system. Furthermore, the ratio of the Fermi momentum  $\hbar k_F$  to  $v_F$  also depends on  $n$ . While  $k_F$  is proportional to  $\sqrt{n}$ ,  $v_F$  does not depend on  $n$  in a Dirac-cone system. These lead to  $\mu \propto 1/n$  and qualitatively explain the negative density dependence, which is not expected for parabolic band dispersion. On the other hand, the mobilities shown in Fig. 4 appear to have stronger density dependence. In the present puddle model, the density and mobility are assumed to be uniform within each puddle. Scattering at the boundary between puddles is not taken into account. These weaknesses of the model may be responsible for the remaining discrepancy.

#### IV. CONCLUSION

In summary, we have studied the transport properties of ultrathin Bi films grown on a cleaved GaAs (110) surface. The temperature evolution of the sheet resistance demonstrates that crystalline flat films, which are similar to those revealed by STM experiments [18], are formed by the two-step growth process. The smallness of  $R_{\text{sq}}$  is attributed to the cancellation of electron and hole contributions and demonstrates the electron-hole symmetry. The experimental results including the linearlike positive magnetoresistance and carrier-density dependence of mobility are explained in terms of the formation of Dirac cones, which are simulated by the tight-binding method and expected to be accidental ones in the presence of strong spin-orbit coupling.

#### ACKNOWLEDGMENTS

This work was supported by JSPS KAKENHI Grants No. JP19H01849 and No. JP20K03816.

- [1] S. Murakami, *Phys. Rev. Lett.* **97**, 236805 (2006).  
 [2] T. Hirahara, G. Bihlmayer, Y. Sakamoto, M. Yamada, H. Miyazaki, S. I. Kimura, S. Blügel, and S. Hasegawa, *Phys. Rev. Lett.* **107**, 166801 (2011).

- [3] F. Yang, L. Miao, Z. F. Wang, M.-Y. Yao, F. Zhu, Y. R. Song, M.-X. Wang, J.-P. Xu, A. V. Fedorov, Z. Sun, G. B. Zhang, C. Liu, F. Liu, D. Qian, C. L. Gao, and J.-F. Jia, *Phys. Rev. Lett.* **109**, 016801 (2012).

- [4] C. Sabater, D. Gosálbez-Martínez, J. Fernández-Rossier, J. G. Rodrigo, C. Untiedt, and J. J. Palacios, *Phys. Rev. Lett.* **110**, 176802 (2013).
- [5] T. Hirahara, T. Nagao, I. Matsuda, G. Bihlmayer, E. V. Chulkov, Y. M. Koroteev, P. M. Echenique, M. Saito, and S. Hasegawa, *Phys. Rev. Lett.* **97**, 146803 (2006).
- [6] A. Takayama, T. Sato, S. Souma, and T. Takahashi, *Phys. Rev. Lett.* **106**, 166401 (2011).
- [7] D. Lükermann, S. Sologub, H. Pfürer, and C. Tegenkamp, *Phys. Rev. B* **83**, 245425 (2011).
- [8] A. Takayama, T. Sato, S. Souma, T. Oguchi, and T. Takahashi, *Nano Lett.* **12**, 1776 (2012).
- [9] S. Xiao, D. Wei, and X. Jin, *Phys. Rev. Lett.* **109**, 166805 (2012).
- [10] M. Aitani, T. Hirahara, S. Ichinokura, M. Hanaduka, D. Shin, and S. Hasegawa, *Phys. Rev. Lett.* **113**, 206802 (2014).
- [11] T. Hirahara, T. Shirai, T. Hajiri, M. Matsunami, K. Tanaka, S. Kimura, S. Hasegawa, and K. Kobayashi, *Phys. Rev. Lett.* **115**, 106803 (2015).
- [12] H. Du, X. Sun, X. Liu, X. Wu, J. Wang, M. Tian, A. Zhao, Y. Luo, J. Yang, B. Wang, and J. G. Hou, *Nat. Commun.* **7**, 10814 (2016).
- [13] S. Ito, B. Feng, M. Arita, A. Takayama, R.-Y. Liu, T. Someya, W.-C. Chen, T. Iimori, H. Namatame, M. Taniguchi, C.-M. Cheng, S.-J. Tang, F. Komori, K. Kobayashi, T.-C. Chiang, and I. Matsuda, *Phys. Rev. Lett.* **117**, 236402 (2016).
- [14] S. Ito, M. Arita, J. Haruyama, B. Feng, W.-C. Chen, H. Namatame, M. Taniguchi, C.-M. Cheng, G. Bian, S.-J. Tang, T.-C. Chiang, O. Sugino, F. Komori, and I. Matsuda, *Sci. Adv.* **6**, eaaz5015 (2020).
- [15] G. Bian, X. Wang, T. Miller, T.-C. Chiang, P. J. Kowalczyk, O. Mahapatra, and S. A. Brown, *Phys. Rev. B* **90**, 195409 (2014).
- [16] Y. Lu, W. Xu, M. Zeng, G. Yao, L. Shen, M. Yang, Z. Luo, F. Pan, K. Wu, T. Das, P. He, J. Jiang, J. Martin, Y.-P. Feng, H. Lin, and X.-S. Wang, *Nano Lett.* **15**, 80 (2015).
- [17] J. C. Patrin, Y. Z. Li, M. Chander, and J. H. Weaver, *Phys. Rev. B* **46**, 10221 (1992).
- [18] J. C. Patrin, Y. Z. Li, M. Chander, and J. H. Weaver, *J. Vac. Sci. Technol. A* **11**, 2073 (1993).
- [19] See Supplemental Material at <http://link.aps.org/supplemental/10.1103/PhysRevB.105.205434> for the placement of electrodes, magnetoresistance data on a 1.8-nm-thick film annealed to only 100 K, electric-field doping experiments, current-direction dependence of  $R_{sq}$ , calculations of  $R_H$  for various combinations of the parameters, and tight-binding calculations of the band structure of pseudocubic (110) bilayers.
- [20] T. Sekihara, R. Masutomi, and T. Okamoto, *Phys. Rev. Lett.* **111**, 057005 (2013).
- [21] T. Sekihara, T. Miyake, R. Masutomi, and T. Okamoto, *J. Phys. Soc. Jpn.* **84**, 064710 (2015).
- [22] R. Masutomi and T. Okamoto, *Appl. Phys. Lett.* **106**, 251602 (2015).
- [23] M. Niwata, R. Masutomi, and T. Okamoto, *Phys. Rev. Lett.* **119**, 257001 (2017).
- [24] R. Masutomi, T. Okamoto, and Y. Yanase, *Phys. Rev. B* **101**, 184502 (2020).
- [25] D. B. Haviland, Y. Liu, and A. M. Goldman, *Phys. Rev. Lett.* **62**, 2180 (1989).
- [26] W. Buckel, *Z. Phys.* **154**, 474 (1959).
- [27] T. Hamada, K. Yamakawa, and F. E. Fujita, *J. Phys. F: Met. Phys.* **11**, 657 (1981).
- [28] N. W. Ashcroft and N. D. Mermin, *Solid State Physics* (Saunders College Publishing, New York, 1976).
- [29] D. L. Partin, J. Heremans, D. T. Morelli, C. M. Thrush, C. H. Olk, and T. A. Perry, *Phys. Rev. B* **38**, 3818 (1988).
- [30] G. Song, M. Ranjbar, and R. A. Kiehl, *Commun. Phys.* **2**, 65 (2019).
- [31] J. Martin, N. Akerman, G. Ulbricht, T. Lohmann, J. H. Smet, K. von Klitzing, and A. Yacoby, *Nat. Phys.* **4**, 144 (2008).
- [32] Y. Zhang, V. W. Brar, C. Girit, A. Zettl, and M. F. Crommie, *Nat. Phys.* **5**, 722 (2009).
- [33] K. Asano and C. Hotta, *Phys. Rev. B* **83**, 245125 (2011).
- [34] N. Tajima, A. Ebina-Tajima, M. Tamura, Y. Nishio, and K. Kajita, *J. Phys. Soc. Jpn.* **71**, 1832 (2002).
- [35] A. Kobayashi, S. Katayama, Y. Suzumura, and H. Fukuyama, *J. Phys. Soc. Jpn.* **76**, 034711 (2007).
- [36] N. Tajima, S. Sugawara, R. Kato, Y. Nishio, and K. Kajita, *Phys. Rev. Lett.* **102**, 176403 (2009).
- [37] R. P. Tiwari and D. Stroud, *Phys. Rev. B* **79**, 165408 (2009).
- [38] D. Stroud, *Phys. Rev. B* **12**, 3368 (1975).
- [39] V. Guttal and D. Stroud, *Phys. Rev. B* **71**, 201304(R) (2005).
- [40] S. Cho and M. S. Fuhrer, *Phys. Rev. B* **77**, 081402(R) (2008).